Supplementary Information for

Label-free deep profiling of the tumor microenvironment

Sixian You[1,2,*], Eric J. Chaney[1], Haohua Tu[1], Yi Sun[3], Saurabh Sinha[4,5,6], Stephen A. Boppart[1,2,3,5,6]

[1]Beckman Institute for Advanced Science and Technology, University of Illinois at Urbana-Champaign

[2]Department of Bioengineering, University of Illinois at Urbana-Champaign

[3]Department of Electrical and Computer Engineering, University of Illinois at Urbana-Champaign

[4]Departement of Computer Science, University of Illinois at Urbana-Champaign

[5]Cancer Center at Illinois, University of Illinois at Urbana-Champaign

[6]Carle Illinois College of Medicine, University of Illinois at Urbana-Champaign

[*]Current affiliation: Electrical Engineering and Computer Science, Massachusetts Institute of Technology

Corresponding author: Stephen A. Boppart

Email: boppart@illinois.edu

This PDF file includes:

Supplementary Figure S1 and S2

Supplementary Table S1 and S2

Supplementary Note

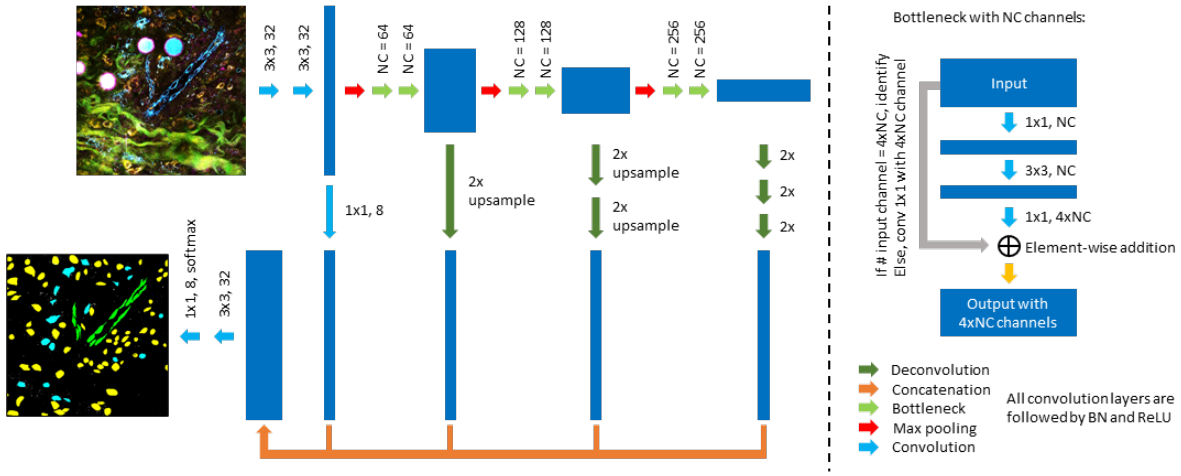

Supplementary Figure S1. Detailed structure of the segmentation network.

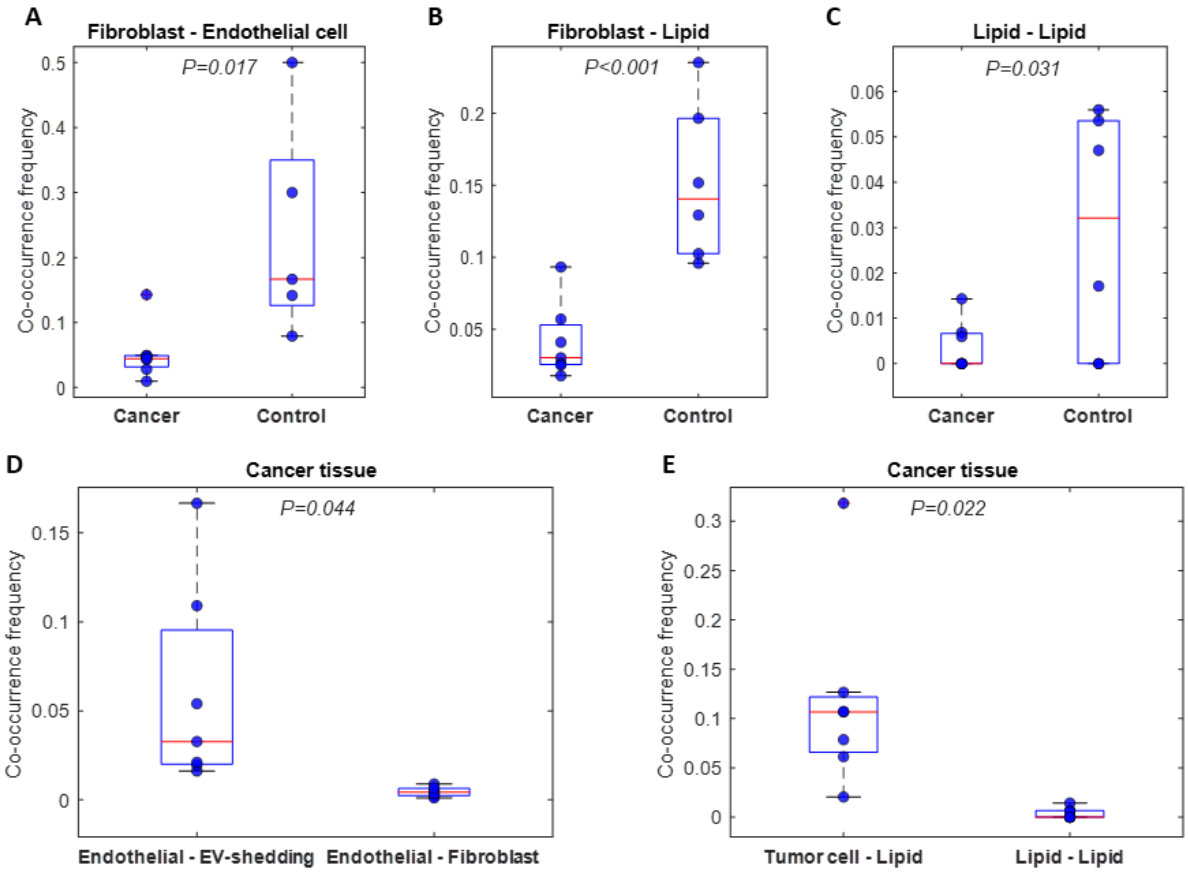

Supplementary Figure S2. Comparison of the co-occurrence frequency between cell types. A-C. Control group shows higher association between fibroblasts and endothelial cells (A), fibroblasts and lipids (B), and the clustering frequency of lipids (C), compared to the cancer group. D. Cancer tissue shows higher co-occurrence between endothelial cells and EV-shedding stromal cells than the normally associated pairs of endothelial cells and fibroblasts. E. Cancer tissue shows higher association between tumor cells and lipids than the normally self-clustered lipids. The co-occurrence frequency between cell type AB is computed by counting the frequency of having cell type B as the nearest neighbor of cell type A, divided by the frequency of cell type B at the imaging site. *P* values in A, B, C were computed using the two-sample Student's t-test based on 6 imaging sites from 3 control animals and 7 imaging sites from 3 tumor-bearing animals. *P* values in D, E were computed using a paired Student's t-test based on the 7 imaging sites from 3 tumor-bearing animals.

Table S1. Segmentation accuracy for each class.

Class/Metric	Precision	Recall	F1 Score
Tumor cell	0.94	0.89	0.92
Fibroblast	0.82	0.89	0.85
Endothelial cell	0.94	0.79	0.86
Lymphocyte	0.83	0.98	0.9
EV-shedding stroma cell	0.87	0.89	0.88
Blood	0.84	0.97	0.9
Lipid	0.99	0.86	0.92
EV	0.91	0.93	0.92

Table S2. Average features of cells in cancer tissues (3 animals) and normal tissues (3 animals).

Cancer

Average value/Cell type	Tumor cell (n=2776)	Fibroblast (n=3924)	Endothelial cell (n=558)	Lymphocyte (n=279)	EV-shedding stroma cell (n=1176)	Lipid (n=956)
Diameter (μm)	13.16 [12.89, 13.44]	16.63 [16.36, 16.9]	20.98 [18.94, 23.25]	9.74 [9.4, 10.12]	17.71 [17.09, 18.34]	34.34 [32.21, 36.59]
Symmetry	1.69 [1.67, 1.71]	1.76 [1.74, 1.79]	2.11 [2.02, 2.21]	1.56 [1.48, 1.67]	1.97 [1.92, 2.02]	1.63 [1.59, 1.67]
Area (μm^2)	74.55 [71.53, 77.72]	120.63 [117.19, 124.17]	178.33 [139.34, 224.71]	45.62 [43.07, 48.35]	119.08 [110.59, 127.82]	975.63 [854.89, 1110.03]
Perimeter (μm)	43.3 [42.07, 44.62]	51.54 [50.62, 52.47]	72.88 [64.1, 82.73]	29.9 [28.71, 31.22]	57.78 [55.33, 60.33]	119.14 [110.73, 128.25]
Roundness	0.59 [0.58, 0.6]	0.57 [0.56, 0.57]	0.43 [0.41, 0.44]	0.69 [0.66, 0.71]	0.47 [0.46, 0.48]	0.55 [0.54, 0.56]
Irregularity	0.28 [0.27, 0.28]	0.29 [0.28, 0.29]	0.34 [0.33, 0.35]	0.23 [0.22, 0.25]	0.33 [0.33, 0.34]	0.25 [0.24, 0.26]
FAD/(FAD+NAD(P)H)	0.93 [0.92, 0.93]	0.94 [0.94, 0.95]	0.76 [0.76, 0.77]	0.88 [0.87, 0.89]	0.68 [0.67, 0.68]	0.79 [0.78, 0.8]
IntensityTHG	22.99 [22.32, 23.69]	19.77 [19.31, 20.25]	21.58 [20.59, 22.61]	42.84 [40.14, 45.66]	22.47 [21.5, 23.5]	49.12 [46.03, 52.3]

Control

Average value/Cell type	Tumor cell (n=NA)	Fibroblast (n=3059)	Endothelial cell (n=258)	Lymphocyte (n=157)	EV-shedding stroma cell (n=NA)	Lipid (n=495)
Diameter (μm)	NA	15.75 [15.46, 16.04]	25.66 [22.17, 29.58]	11.24 [10.55, 11.98]	NA	44.1 [39.4, 49.49]
Symmetry	NA	1.96 [1.93, 2]	2.28 [2.13, 2.44]	1.72 [1.62, 1.82]	NA	1.55 [1.5, 1.6]
Area (μm^2)	NA	92.14 [89.35, 95.08]	179.45 [141.55, 223.7]	50.24 [46.18, 54.73]	NA	2385.78 [1585.56, 3681.4]
Perimeter (μm)	NA	46.22 [45.21, 47.28]	93.62 [78.25, 111.29]	35.05 [32.85, 37.37]	NA	168.6 [135.52, 217.88]
Roundness	NA	0.59 [0.58, 0.6]	0.37 [0.34, 0.39]	0.57 [0.54, 0.6]	NA	0.61 [0.6, 0.63]
Irregularity	NA	0.3 [0.3, 0.3]	0.36 [0.35, 0.38]	0.29 [0.27, 0.31]	NA	0.21 [0.2, 0.22]
FAD/(FAD+NAD(P)H)	NA	0.96 [0.95, 0.96]	0.85 [0.85, 0.86]	0.92 [0.91, 0.93]	NA	0.72 [0.7, 0.73]
IntensityTHG	NA	23.47 [22.87, 24.1]	23.26 [22.13, 24.45]	47.91 [43.81, 52.18]	NA	36.47 [33.49, 39.6]

Note: Confidence intervals were computed by bootstrap. The data is reported in the form of "average and its 95% confidence interval".

Supplementary Note: Training the deep neural network (DNN)

For the task of multiclass pixel-level segmentation, 226 image patches (128 by 128 pixels) were used for training, 16 image patches (128 by 128 pixels) from were used for validation, and 22 image patches (128 by 128 pixels) from were used for testing. As with most biomedical image analysis task, the limited training data presents a challenge for using DNN for cell segmentation. To reduce overfitting and improve segmentation accuracy, we used the following methods. (a) We followed the modified U-Net (1) architecture by Yang et al. (2), where ResNet bottleneck design with identify shortcuts and batch normalization are applied on top of the standard U-Net (1) (Supplementary Figure S1 as shown below). Bottleneck design leads to better parameter efficiency (maintaining same number of feature channels while reducing number of parameters) and batch normalization leads to more stable training. (b) Through experiments on the validation set, we found the best F1 score can be achieved by removing the last two scale blocks from the architecture in Yang et al.'s work (see more details of the model architect design in Supplementary Figure S1). By removing the last two blocks, we reduce a significant amount of parameters in the network and thus reduce the risk of overfitting. (c) We adopted standard image augmentations (e.g. rotation, flipping, and cropping) to further reduce overfitting. Finally, our evaluation on the test set (Table S1) shows our network can generalize well to unseen images.

Reference

1. Ronneberger O, Fischer P, Brox T. U-Net: convolutional networks for biomedical image segmentation. Med Image Comput Comput Interv — MICCAI 2015 [Internet]. 2015;234–41. Available from: http://arxiv.org/abs/1505.04597%5Cnhttp://link.springer.com/10.1007/978-3-319-24574-4_28

2. Yang L, Zhang Y, Chen J, Zhang S, Chen DZ. Suggestive annotation: A deep active learning framework for biomedical image segmentation. Lect Notes Comput Sci (including Subser Lect Notes Artif Intell Lect Notes Bioinformatics). 2017.